https://doi.org/10.5194/egusphere-2026-1001
Preprint. Discussion started: 7 April 2026

Applied Machine Learning for Flood Susceptibility Mapping in the Loukkos Basin (Northern Morocco): Validation Using the February 2026 Ksar El Kebir Flood Event

Oussama Mekkaoui[1], Moad Morarech[1], Tarik Bouramtane[2], Hamza Akka[3]

[1]Laboratory of Applied and Marine Geosciences, Geotechnics and Geohazards (LR3G), Faculty of Sciences of Tetouan, University Abdelmalek Essaadi, Tetouan 93030, Morocco
[2]Geoscience, Water and Environment Laboratory, Faculty of Sciences, Mohammed V University in Rabat, Avenue Ibn Batouta, Rabat 10100, Morocco
[3]Laboratory, Research & Development in Applied Geosciences, Faculty of Science and Techniques Tangier, University of Abdelmalek Essaadi, Tangier 90000, Morocco

Correspondence to: Oussama Mekkaoui (oussama.mekkaoui@etu.uae.ac.ma)

Abstract. Flooding is a recurrent hazard in northern Morocco, where low-lying alluvial plains, strong river–floodplain connectivity, and winter storm sequences combine to produce damaging floods. This study develops an event-informed flood susceptibility assessment for the Loukkos Basin (Ksar El Kebir–Larache floodplain) by integrating satellite-derived flood evidence with geomorphometric and hydro-climatic predictors in a machine-learning framework. A binary flood inventory was derived from Sentinel-1 SAR change detection by contrasting pre-flood (October–November 2022) and flood-phase acquisitions (December 2022), and was validated using Sentinel-2 optical observations and field checks. Nine conditioning factors (elevation, slope, aspect, curvature, distance to rivers, drainage density, TWI, TPI, and CHIRPS-based rainfall) were compiled and standardized on a 10 m grid. Model training used a balanced sample of 220 points (110 flooded/110 non-flooded) and was evaluated with a repeated hold-out strategy (10 iterations; 80% training/20% testing) using accuracy, precision, recall, and F1-score. Both Random Forest (RF) and Multilayer Perceptron (MLP) produced coherent susceptibility patterns, with the highest classes concentrated along the Loukkos river corridor and downstream floodplains. Mean test performance indicates strong generalization, with MLP outperforming RF (accuracy ≈ 0.909 vs. 0.864; F1 ≈ 0.909 vs. 0.870). Jackknife sensitivity analysis identifies elevation as the leading control for both models, while RF emphasizes terrain metrics (slope, drainage density) and MLP assigns a more balanced importance to topography and hydrological drivers (TPI, rainfall, distance to channel). Notably, flooded areas observed during the January–February 2026 flood episode (Sentinel imagery dated 14 February 2026) largely coincide with zones mapped as high susceptibility, providing an independent, qualitative post-study consistency check. The resulting maps offer a practical inspection tool to support land-use planning and prioritization of mitigation actions across the most flood-prone sectors of the Loukkos Basin.

1 Introduction

Flooding is widely recognized as one of the most pervasive and damaging natural hazards because it combines high physical occurrence with rapidly increasing exposure of people, infrastructure, and economic activity in flood-prone environments (Organization, 2021; UNDRR, 2020). Global disaster records indicate that flood risk is not only a function of hydro-climatic extremes but also of where and how societies develop, since changes in land use, settlement patterns, and protective capacity directly reshape vulnerability and exposure (Rahman et al., 2016; UNDRR, 2020). Over recent decades, climate-related hazards have become more prominent in disaster statistics, with floods consistently ranking among the most frequent event types and accounting for substantial socio-economic disruption (Organization, 2021; UNDRR, 2020). In its synthesis of global disaster databases, UNDRR reports that between 2000 and 2019 the number of major flood events more than doubled relative to 1980–1999, alongside broader growth in climate-related disasters and associated losses (UNDRR, 2020). Complementary long-term assessments emphasize the cumulative toll: the WMO's global review documents nearly 12,000

https://doi.org/10.5194/egusphere-2026-1001
Preprint. Discussion started: 7 April 2026

weather-, climate- and water-related disasters between 1970 and 2021, with reported economic losses of about US$4.3 trillion and around 2 million deaths, disproportionately affecting developing countries (Organization, 2021).

A key physical driver shaping contemporary flood hazard is the intensification of the hydrological cycle under anthropogenic warming, which increases the likelihood of heavy precipitation and enhances runoff-generating conditions in many regions (Masson-Delmotte et al., 2021). The IPCC Sixth Assessment Report (AR6) concludes with high confidence that additional warming increases the frequency and intensity of heavy precipitation, implying heightened potential for pluvial and fluvial flooding where hydrological and drainage capacities are exceeded (Masson-Delmotte et al., 2021). At the same time, exposure is increasing because populations and assets continue to expand into inundation-prone areas, meaning that even unchanged hazards can produce higher impacts through growth and concentration of development (Tellman et al., 2021). Satellite-based evidence indicates that the population living in locations with observed inundation increased by tens of millions between 2000 and 2015, underscoring how rapid growth in flood-exposed zones is reshaping global risk (Tellman et al., 2021).

Urbanization and land-use change can further amplify flood occurrence and impacts by increasing impervious surfaces, accelerating runoff, constraining natural storage, and placing critical infrastructure in vulnerable lowlands (Handayani et al., 2020; Miller and Hutchins, 2017). Reviews synthesizing evidence from urban catchments show that climate drivers and urban development act jointly, with changes in rainfall extremes and land-surface properties combining to increase flood likelihood and degrade water quality in many settings (Miller and Hutchins, 2017). Empirical analyses in rapidly urbanizing regions similarly connect land-use/land-cover transitions to increased flood incidence at the basin scale, highlighting the governance challenge of aligning spatial planning with hydrological realities (Handayani et al., 2020). Because floods impose both direct damages (housing, roads, utilities) and indirect losses (service disruption, productivity shocks), the economic implications are substantial and spatially heterogeneous, motivating the need for risk assessments that connect hazard intensity to exposed assets and functions (Chauhan et al., 2023; Svetlana et al., 2015).

Within this context, GIS-based flood risk and susceptibility mapping has become a central component of preparedness and incident management, particularly where dense hydrometric networks or long discharge records are limited (Alexander et al., 2011; Hossain and Meng, 2020a). Local-scale decision support tools can translate hazard and exposure information into operational products for emergency response and planning, including the identification of priority hotspots, vulnerable populations, and critical infrastructure (Alexander et al., 2011). Fine-scale spatial analytics further show that building- and population-level risk patterns can vary markedly within a single urban system, strengthening the case for spatially explicit assessments rather than uniform, coarse zoning (Hossain and Meng, 2020b). In parallel, the increasing availability of Earth observation for disaster management supports more consistent, event-based flood evidence and improved situational awareness, including through coordinated international initiatives for satellite support during crises (Wood and Lauritson, 2000).

In Morocco, flood risk represents a recurrent challenge with measurable national-scale consequences and well-documented catastrophic events (OECD, 2017). National risk governance assessments report modelled average annual flood losses on the order of billions of dirhams, with the potential for much larger losses under rare, high-magnitude events, highlighting both chronic impacts and tail-risk exposure (OECD, 2017). The same assessment documents the severity of historical disasters such as the 1995 Ourika Valley flood, which produced major loss of life and remains a benchmark for risk memory and prevention needs (OECD, 2017). Morocco's flood prevention efforts have included large-scale programs combining structural and non-structural measures, with prioritization across basins and evolving investment patterns that reflect both hazard experience and institutional constraints (OECD, 2017). In northern Morocco, multi-hazard and climate-risk syntheses emphasize that coastal and lowland sectors can concentrate high-risk zones, including areas around Larache and the Loukkos basin, which are highlighted as locations where flood risk intersects with exposure and vulnerability (Agharroud et al., 2023). Regional assessments and social research also show that risk awareness and precautionary behavior vary across

https://doi.org/10.5194/egusphere-2026-1001
Preprint. Discussion started: 7 April 2026

communities in northern Morocco, reinforcing that vulnerability is not only physical but also shaped by perception, preparedness, and local capacity (Ivčević et al., 2020). Local and regional flood studies in the broader Tangier–Tétouan region have therefore increasingly combined spatial analysis and modelling to identify flood-prone areas and drivers, including machine-learning and multivariate approaches in Tangier (Bouramtane et al., 2021; Mekkaoui et al., 2025) and watershed-scale risk mapping and hydraulic modelling in nearby basins such as the Martil watershed (Azouagh et al., 2018; Karrouchi et al., 2016b).

Methodologically, flood susceptibility mapping seeks to estimate the spatial propensity for flooding from the configuration of conditioning factors such as topography, proximity to channels, land cover, and rainfall characteristics, providing actionable prioritization where direct flow records are sparse (Choubin et al., 2019; Mosavi et al., 2018). Alongside expert-based or multi-criteria approaches, machine-learning methods have been increasingly adopted because they can represent non-linear interactions among flood drivers and often improve predictive skill when trained on suitable flood inventories (Breiman, 2001; Mosavi et al., 2018). Ensemble frameworks that combine multiple statistical and ML classifiers have been widely proposed for flood susceptibility assessment, aiming to reduce dependence on a single model structure and to improve robustness across heterogeneous terrain (Choubin et al., 2019). For operational flood modelling and scenario analysis, process-based hydrologic and hydraulic tools (e.g., HEC-HMS/HEC-RAS) are also commonly integrated with GIS to simulate flood extents and support calibration or validation against observed impacts (AL-Hussein et al., 2022; Azouagh et al., 2018; Syarifudin et al., 2022). Across these approaches, the credibility of susceptibility products depends strongly on (i) the quality and representativeness of the flood inventory and (ii) rigorous validation strategies that quantify generalization rather than memorization of a single data split (Fawcett, 2006; Kohavi, 1995).

Despite methodological advances, two issues remain particularly consequential for Moroccan basins: flood inventories are often limited in space and time, and model skill can be overstated when evaluation relies on a single partition of data that may not reflect true out-of-sample performance (Kohavi, 1995; OECD, 2017). This is especially relevant for high-exposure northern basins, where targeted susceptibility products are needed to support prioritization of mitigation and preparedness under evolving climate and land-use pressures (Agharroud et al., 2023). Motivated by these needs, this study develops a flood susceptibility assessment for the Loukkos Basin that is explicitly anchored in remotely sensed flood evidence and designed for reproducible model evaluation (Kohavi, 1995; Wood and Lauritson, 2000). Specifically, we (i) compile a flood inventory from satellite observations of a documented flood episode, (ii) assemble flood-conditioning variables consistent with the basin's hydro-geomorphic setting and available environmental data, and (iii) compare expert-based and machine-learning susceptibility models, including non-linear classifiers (Alexander et al., 2011; Mosavi et al., 2018). To reduce sensitivity to any single training–testing split, we apply repeated hold-out validation across multiple partitions and quantify predictive skill using threshold-independent metrics such as ROC/AUC (Fawcett, 2006; Kohavi, 1995). Finally, we examine the relative contribution of conditioning factors through sensitivity/importance analysis to support interpretable risk communication and operational uptake (Choubin et al., 2019; Hossain and Meng, 2020b). The resulting products aim to provide an evidence-based susceptibility map for a high-concern northern Moroccan basin, an explicit comparison of modelling paradigms relevant to practice, and clearer insight into dominant flood controls that can guide targeted risk reduction (Karrouchi et al., 2016a; OECD, 2017).

2 Study Area and data

2.1 Study Area

The Loukkos Basin is located in northwestern Morocco along the Atlantic margin, approximately between 34°50′N–35°20′N and 6°00′W–5°20′W. It covers about ~3,730 km² and is drained by the Loukkos River, which rises in the Rif Mountains and flows westward to the Atlantic Ocean near Larache (ABHL Agence du Bassin Hydraulique du Loukkos, 2016; Ministère de

https://doi.org/10.5194/egusphere-2026-1001
Preprint. Discussion started: 7 April 2026

l'Équipement et de L'eau, 2023). The river network includes major tributaries such as Oued El Makhazine, Oued Drader, and Oued Khmis, which contribute to rapid catchment-wide runoff generation during winter storms (ABHL Agence du Bassin Hydraulique du Loukkos, 2016).

The basin shows a strong upstream–downstream contrast that is central to flood vulnerability. The northeastern headwaters, around Ouezzane and Ain Dorij, are characterized by steep, dissected relief and narrow valleys, promoting fast runoff concentration and short response times (Martín-Martín et al., 2020). Downstream, the broad and low-gradient alluvial plain, particularly the corridor connecting Ksar El Kebir and Larache, favors overbank flow, flood spreading, and long inundation duration, which increases exposure of agricultural land, settlements, and infrastructure (El Khalki et al., 2020). In the estuarine reach, semi-diurnal tides can modulate water levels and locally hinder drainage during high stages, which may intensify flooding in the lowest plain (Acharki et al., 2023).

The basin experiences a Mediterranean climate with wet winters and dry summers, and a marked seasonal concentration of rainfall. Reported annual precipitation typically exceeds ~700 mm in the northern mountainous zones and decreases toward ~500 mm near coastal and southern sectors (ABHL Agence du Bassin Hydraulique du Loukkos, 2016; El Moçayd et al., 2020). This spatial gradient—combined with multi-day winter storm sequences—supports both flash-type tributary responses upstream and widespread plain inundation downstream during basin-scale events. Geologically, the basin belongs to the Rif domain and is dominated by Meso–Cenozoic formations with alternating marls and calcareous units (Martín-Martín et al., 2020). In the upper basin, marl, sandstone, schist, and limestone outcrops are often mantled by clay-rich soils and colluvial deposits, which can limit infiltration and enhance surface runoff during prolonged wet-season rainfall. In the lower plain, Quaternary alluvial and fluvio-marine deposits over marly/marl-limestone substrata form extensive low-permeability floodplain environments where water can pond and persist after peak flows (El Khalki et al., 2020). Flow regulation is a major component of the basin's functioning, notably through the Oued El Makhazine Dam, which supports irrigation and water supply and influences downstream flood propagation (ABHL Agence du Bassin Hydraulique du Loukkos, 2016; Benchbani et al., 2022; Tramblay, 2012). During very wet seasons, high reservoir filling levels may require controlled releases, which can increase downstream flood hazard when combined with elevated river stages and saturated floodplain conditions.

The basin hosts a shallow aquifer system (Loukkos aquifer), mainly developed in Quaternary alluvial and sandy formations, playing a key role for irrigation and sustaining base flow during dry periods (Boughriba et al., 2010). However, intensified pumping and land-use change are reported to affect recharge dynamics and may reduce buffering capacity under hydrologic extremes (ABHL Agence du Bassin Hydraulique du Loukkos, 2016; Alami and Jilali, 2023; Sarti et al., 2021). This coupling between shallow groundwater, antecedent wetness, and drainage efficiency is especially relevant in the downstream plain where flood vulnerability is highest. Land use is dominated by intensive agriculture in the lower plain, where crops benefit from irrigation supplied by the river system and groundwater (ABHL Agence du Bassin Hydraulique du Loukkos, 2016). Urban growth around Larache, Ksar El Kebir, and Moulay Bousselham has expanded built-up surfaces and increased exposure in low-lying areas (ABHL Agence du Bassin Hydraulique du Loukkos, 2016; El Khalki et al., 2020)). These trends can accelerate runoff, reduce natural flood retention, and amplify flood impacts on housing, transport links, and irrigated perimeters.

The Loukkos plain has experienced recurrent damaging floods, including notable events reported in 2000, 2008, and 2010, with severe impacts on agriculture and infrastructure in low-lying zones (ABHL Agence du Bassin Hydraulique du Loukkos, 2016). Beyond these recent episodes, geomorphological and historical analyses indicate that major inundations have long affected the lower valley and the Ksar El Kebir sector, reflecting the intrinsic susceptibility of the floodplain–estuary system (Benchbani et al., 2022; Tramblay, 2012).

https://doi.org/10.5194/egusphere-2026-1001
Preprint. Discussion started: 7 April 2026

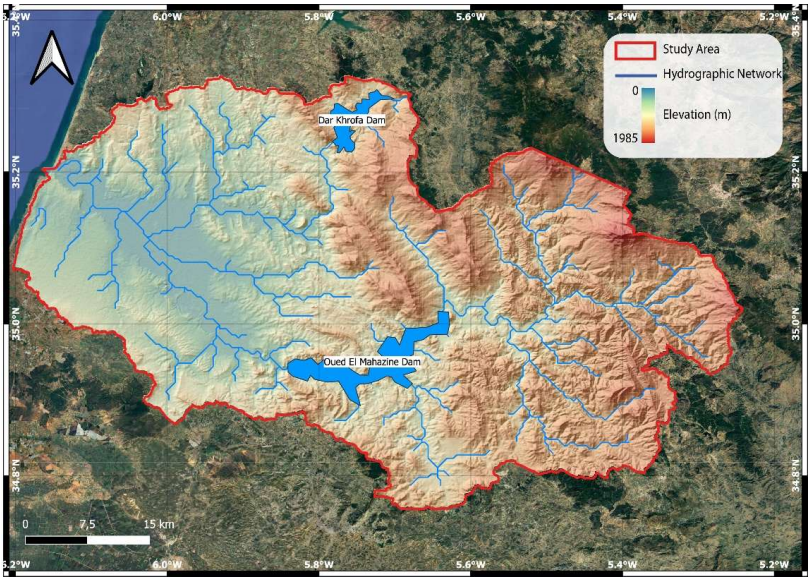

Figure 1. Location of the Loukkos Basin (Northern Morocco) showing the basin boundary, drainage network, and topography (DEM elevation, m). Major hydraulic infrastructures (Dar Khrofa Dam and Oued El Makhazine Dam) are indicated.

The most significant and operationally relevant event for the present study is the late January 2026 flood. During this episode, exceptionally intense and persistent rainfall led to a rapid rise in the Loukkos River, prompting authorities to raise the alert level to its maximum in Ksar El Kebir. The river overtopped its banks, inundating streets and low-lying neighborhoods, disrupting transport and essential services, and forcing large-scale evacuations of residents in the city and surrounding areas. Emergency response measures were activated, including civil protection interventions, temporary shelters, and precautionary restrictions in flood-prone zones. The event was further documented through an activation of the International Charter: Space and Major Disasters (29–30 January 2026), which reported unusually wet seasonal conditions across northern Morocco and indicated that reservoir levels had reached or exceeded capacity. As a result, controlled discharges from upstream reservoirs were implemented to ensure dam safety, contributing to increased downstream flows and aggravating flood propagation along the Loukkos floodplain. According to multiple media and institutional sources, the January 2026 flood represents one of the most severe hydrological events recorded in the Loukkos Basin in recent decades.

2.2 Flood Inventory Map

Flood maps represent a fundamental component in flood risk assessment, serving as the basis for identifying and extracting samples of flooded and non-flooded areas that are essential for developing accurate flood susceptibility models (Hitouri et al., 2024; Nusit et al., 2025). The reliability and predictive performance of these models are directly influenced by the accuracy of the flood inventory dataset (Sellami et al., 2022). In the Loukkos Basin, located in northern Morocco, flood events are primarily driven by intense and short-duration rainfall, high drainage density, and the combined influence of Atlantic humidity and the basin's complex topography (El Falah et al., 2021; Karrouchi et al., 2016a; Mekkaoui et al., 2025). These floods often occur suddenly and with significant spatial variability, making precise flood mapping an indispensable step in susceptibility analysis (Nusit et al., 2025). Synthetic Aperture Radar (SAR) imagery, particularly from the Sentinel-1 mission, has proven highly effective for flood mapping and monitoring due to its ability to penetrate cloud cover and operate independently of daylight conditions, ensuring consistent observations during and after extreme hydro-meteorological events (Cao et al., 2019; Zhao et al., 2024). This technique exploits the sensitivity of SAR backscatter to surface roughness and moisture content, both of which change markedly during flooding (Feizbahr et al., 2025; Zhao et al., 2024). Sentinel-1

https://doi.org/10.5194/egusphere-2026-1001
Preprint. Discussion started: 7 April 2026

operates in the C-band (5.405 GHz) and provides dual-polarization data—VV (vertical–vertical) and VH (vertical–horizontal). In this study, VH polarization was selected for its greater sensitivity to volume scattering, enabling improved detection of inundated vegetation and open water surfaces (Badillo-Rivera et al., 2025; Kim et al., 2025; Monika and Berezowski, 2025).

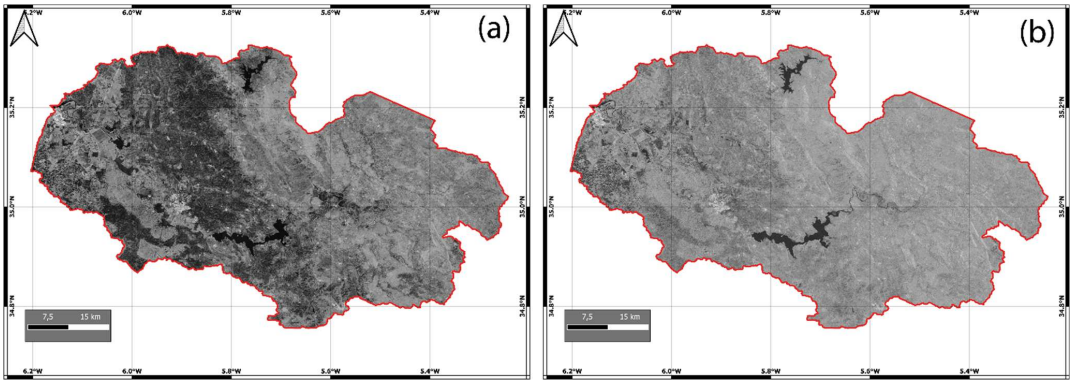

Figure 2. The Sentinel-1 SAR images for two distinct periods: (a) pre-flood phase (October 1–November 28, 2022) representing normal surface conditions, (b) a flood phase (December 14–28, 2022) capturing the extent of inundation

For this analysis, Sentinel-1 SAR images were acquired for two distinct temporal periods over the Loukkos Basin: a pre-flood phase (October 1–November 28, 2022), representing baseline conditions, and a flood phase (December 14–28, 2022), corresponding to the main flood event recorded in the basin (Figure 2). (Ministère de l'Équipement et de L'eau, 2023). A change detection approach was employed by comparing backscatter intensity values between the two phases. Pixels exhibiting a decrease in backscatter below a defined threshold were classified as flooded (value = 1), whereas those above the threshold were classified as non-flooded (value = 0) (Abbasi et al., 2023; Hitouri et al., 2024; Tazmul Islam and Meng, 2022) . The resulting binary flood map was visualized using a colour scheme in which blue represents flooded areas and green represents non-flooded zones (Figure 3). The classification results were validated using Sentinel-2 optical imagery and field observations collected across lowland agricultural areas and near the Loukkos River to verify the spatial extent and accuracy of the detected inundation.

From the finalized flood inventory map, 220 data points were randomly extracted across the watershed to construct the modelling dataset, comprising 110 flooded and 110 non-flooded points (Figure 3). This balanced sampling approach was adopted to ensure that both classes were equally represented during the training of machine learning models. Although this balance does not mirror the real spatial distribution where non-flooded areas dominate it is a standard practice in flood susceptibility modelling to reduce model bias toward the majority class and to enhance the algorithm's capacity to recognize flooded pixels accurately (Asghar Rostami et al., 2025). The resulting dataset thus provides a robust foundation for subsequent flood susceptibility modelling and validation within the Loukkos Basin, contributing to a better understanding of flood dynamics in Morocco's humid semiarid transition zone.

https://doi.org/10.5194/egusphere-2026-1001
Preprint. Discussion started: 7 April 2026

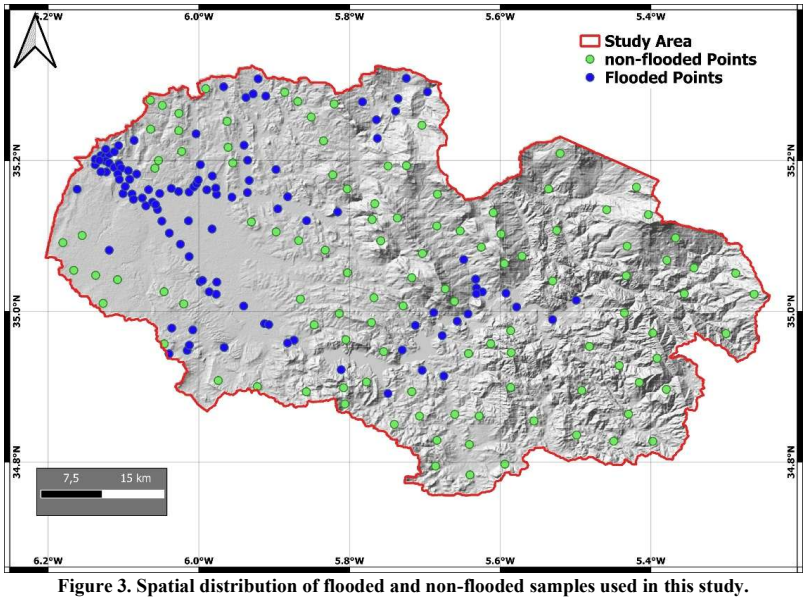

Figure 3. Spatial distribution of flooded and non-flooded samples used in this study.

2.3 Factors influencing flooding

This section describes the selection and relevance of the conditioning factors used for flood susceptibility assessment. The choice of variables was guided by data availability, their physical significance in flood-generating processes, and a review of relevant literature to ensure consistency with previous studies (Bouramtane et al., 2021; Mekkaoui et al., 2025). This systematic approach ensures that all selected factors are both publicly accessible and scientifically validated. Spatial analysis, preprocessing, and derivation of input variables were carried out using QGIS software. Nine flood-conditioning factors were retained: elevation, slope, aspect, curvature, distance from rivers, drainage density, Topographic Wetness Index (TWI), Topographic Position Index (TPI), and rainfall. The spatial distribution of these factors is illustrated in Figure (4). To ensure spatial consistency, all datasets were resampled and converted to a uniform 10 × 10 m grid resolution, corresponding to the resolution of the Digital Elevation Model, prior to analysis.

The elevation (Figure 4-a) of the study area ranges from 0 to 1,985 m, with most parts located at low altitudes. It was obtained from the Digital Elevation Model (DEM) and represents a key factor influencing flood susceptibility. Low-lying areas tend to accumulate runoff and are therefore more vulnerable to flooding during intense rainfall, while higher altitudes facilitate faster drainage and reduce inundation risk. This variation in elevation strongly affects the spatial distribution of flood-prone zones across the study area.

Slope (Figure 4-b) influences flood dynamics by controlling the speed and direction of surface runoff. Steeper slopes promote rapid water flow and reduce water accumulation, while flatter areas increase the likelihood of flooding. The slope angle, ranging from 0° to 82°, was derived from the Digital Elevation Model (DEM) using QGIS tools, which calculate the maximum rate of elevation change for each cell. As a major physiographic factor, slope directly affects runoff velocity and sediment transport, playing a crucial role in flood susceptibility assessment.

Exposition (Figure 4-c) represents the orientation of the slope and indirectly influences flood susceptibility by affecting rainfall exposure, solar radiation, evapotranspiration, and vegetation cover. It determines microclimatic conditions such as moisture retention and surface drying, which can modify runoff behavior. Aspect values, ranging from 0° to 360°, indicate slope direction starting from North (0°) and progressing clockwise. This parameter was derived from the Digital Elevation Model (DEM) using QGIS tools.

https://doi.org/10.5194/egusphere-2026-1001
Preprint. Discussion started: 7 April 2026

Curvature ((Figure 4-d), unitless) describes the shape of the land surface and significantly influences surface runoff and flood susceptibility. It was derived from the Digital Elevation Model (DEM) using QGIS tools. Positive curvature values indicate concave areas where water tends to accumulate, negative values represent convex zones where water disperses, and values near zero correspond to flat surfaces. This parameter helps identify areas prone to water concentration and potential flooding.

Distance from channel (Figure 4-e) is a crucial factor influencing flood susceptibility, as areas closer to rivers are more exposed to overflow and inundation. This parameter, expressed in meters (m), was generated using GIS software, which calculates the straight-line distance of each pixel from the nearest river channel. Shorter distances indicate higher flood potential, while greater distances generally correspond to lower susceptibility.

Drainage density (km/km2, Figure 4-f) represents the length of watercourses in kilometers per unit area in square kilometers (km2). It reflects the permeability of the soil surface and the infiltration rate, and therefore controls the intensity of runoff, which is directly linked to flooding. It was calculated from the drainage network using the linear density tool in the QGIS software.

The Topographic Wetness Index TWI ((Figure 4-g), unitless) quantifies the tendency of water to accumulate at each point in the watershed, reflecting the influence of topography on runoff generation and soil saturation. It represents the potential for surface flow and moisture concentration, with higher values indicating wetter conditions. TWI typically ranges from 2–6 in steep, well-drained areas and exceeds 10 in flat or low-lying zones with greater water accumulation potential. This parameter was generated using GRASS GIS 7.6.1 tools.

The Topographic Position Index TPI ((Figure 5-h), unitless) indicates the upper and lower parts of the landscape, i.e., the difference in altitude of each cell in relation to the average altitude of the surrounding cells. Positive values indicate areas above the surrounding cells, i.e., ridges, while values near zero generally represent flat terrains, and finally negative values indicate areas below the surrounding cells, i.e., valleys, this parameter was generated using GIS software.

Rainfall (Figure 4-i) mapping for the period 2020–2024 was carried out using CHIRPS (Climate Hazards Group InfraRed Precipitation with Station Data) within the Google Earth Engine (GEE) platform. Daily precipitation data were aggregated into monthly totals and then summed to obtain cumulative rainfall over the five-year period. The resulting rainfall map reveals clear spatial variability in precipitation intensity across the study area. These variations are closely related to topographic influences and prevailing atmospheric circulation patterns. Rainfall values, expressed in millimetres (mm), range from 2,339 mm to 4,299 mm. Such spatial differences provide essential information for understanding local hydrological processes, supporting flood risk assessment, and analysing climate variability and change in the region.

3. Materials and Methods

3.1 Multilayer Perceptron (MLP) Algorithm

The Multilayer Perceptron (MLP) is a type of artificial neural network (ANN) designed to model complex nonlinear relationships between input and output variables. It consists of an input layer, one or more hidden layers, and an output layer, with each layer composed of interconnected processing nodes called neurons (Chan et al., 2023). Each neuron processes incoming signals by applying weighted sums followed by nonlinear activation functions such as the sigmoid, hyperbolic tangent, or Rectified Linear Unit (ReLU) (Chen et al., 2015; Zhao et al., 2024). During the training phase, MLP adjusts the connection weights through the backpropagation algorithm to minimize prediction error using optimization methods such as gradient descent. In flood susceptibility modelling, MLP is particularly effective for learning complex, nonlinear interactions among multiple hydrological, topographic, and environmental variables (Ahmadlou et al., 2021; Riazi et al., 2023). It can integrate diverse datasets, including remote sensing indices, rainfall, soil characteristics, and terrain attributes, to predict flood-prone areas with high accuracy (Haribabu et al., 2021; Mosavi et al., 2018). The strength of MLP lies in its ability to

https://doi.org/10.5194/egusphere-2026-1001
Preprint. Discussion started: 7 April 2026

285 capture subtle spatial and temporal patterns that are often missed by traditional statistical models. However, it requires careful tuning of parameters such as the number of hidden layers, learning rate, and activation functions to avoid overfitting and ensure model stability. Despite these challenges, MLP has proven to be a powerful and flexible tool for flood susceptibility assessment and environmental hazard prediction when combined with GIS and remote sensing techniques (Bouramtane et al., 2022b; Pham et al., 2018).

290

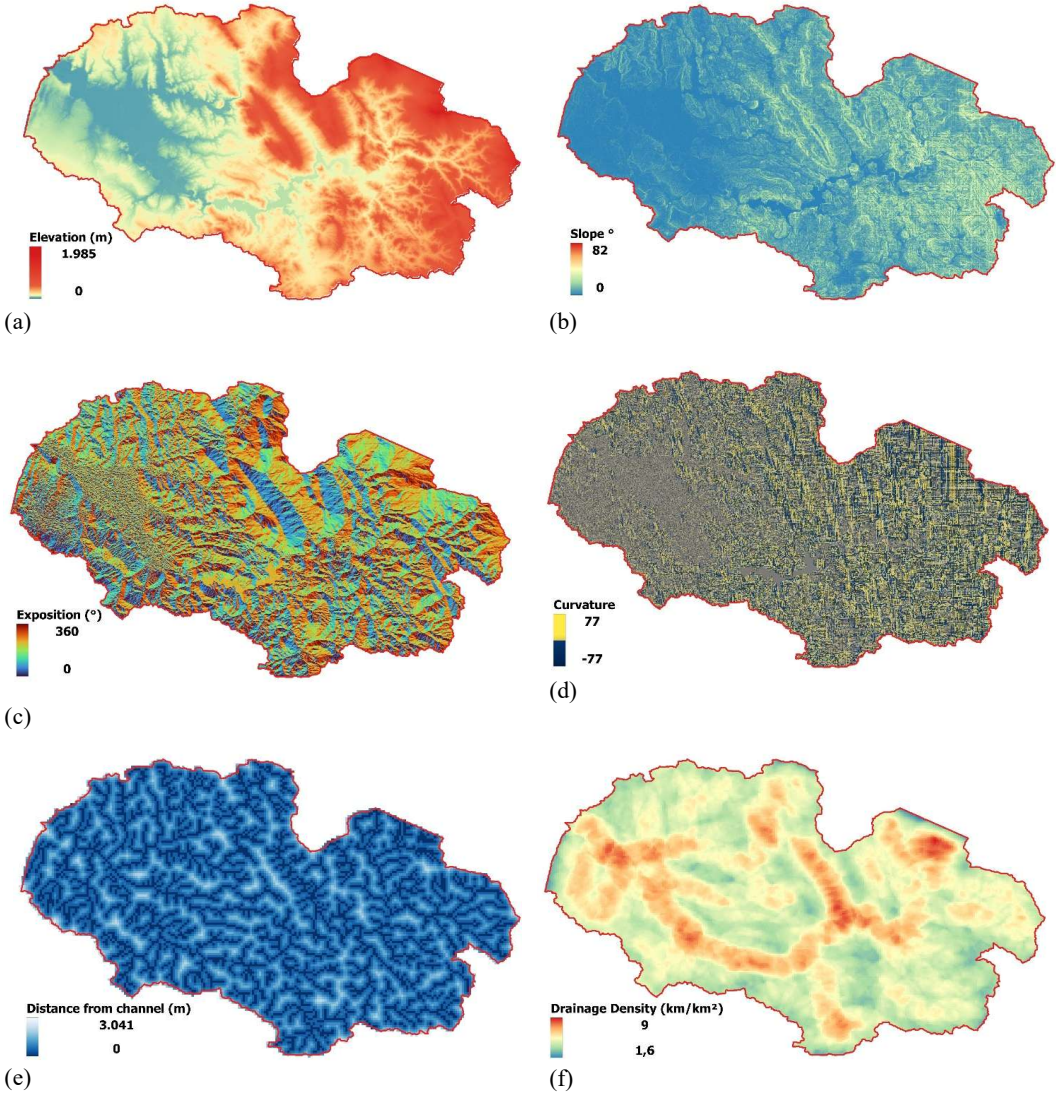

https://doi.org/10.5194/egusphere-2026-1001
Preprint. Discussion started: 7 April 2026

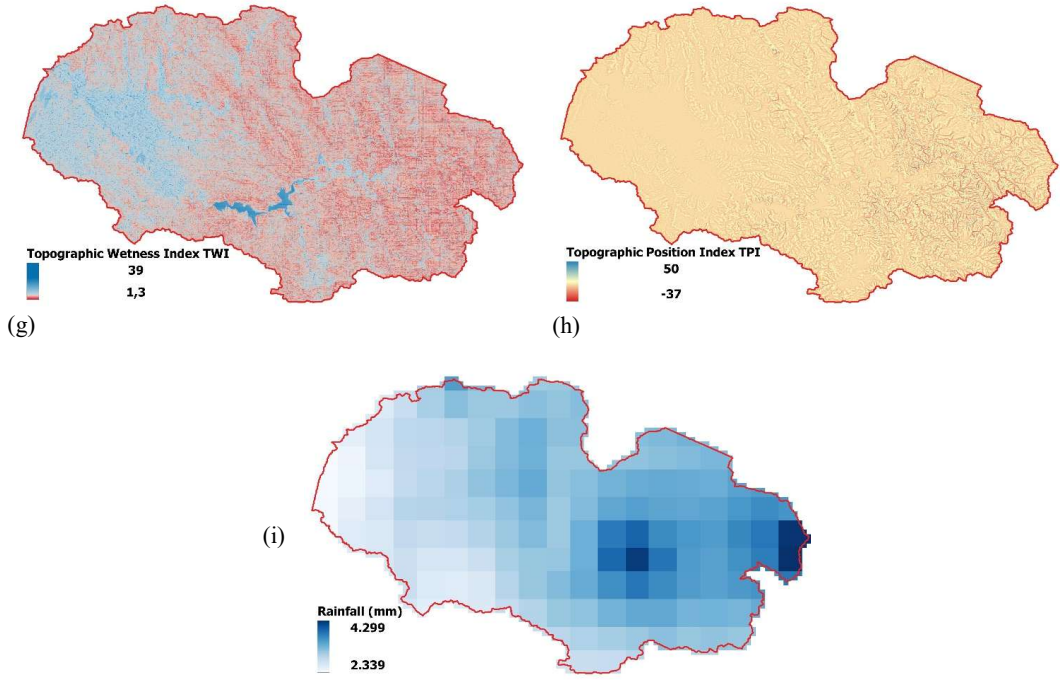

Figure 4. Maps of Flood conditioning factors of the study area (a) Elevation, (b) Slope, (c) Exposition, (d) Curvature, (e) Topographic Position Index (TPI), (f) Topographic Wetness Index (TWI), (g) Drainage density, (h) Distance to channel, (i) Rainfall.

3.2 Random Forest (RF) Algorithm

The Random Forest (RF) algorithm, introduced by Breiman (Breiman, 2001), is an ensemble learning technique that builds multiple decision trees using random subsets of both the data and predictor variables. This dual randomization process, combining bootstrap aggregation or bagging with random feature selection, enhances model robustness and prevents overfitting (Ganjirad and Delavar, 2023). Each tree contributes a vote, and the final prediction is determined by the majority class for classification or by averaging for regression (Breiman, 2001; Wahba et al., 2024). RF is a nonlinear and nonparametric method capable of modelling complex relationships between variables without requiring statistical assumptions about data distribution (Halder et al., 2024). It performs well with large and high-dimensional datasets, maintains strong predictive accuracy, and is resistant to noise and outliers (Al-Aizari et al., 2024). In flood modelling, RF effectively integrates diverse hydrological and environmental parameters such as elevation, slope, rainfall, and drainage density to identify key factors influencing flood occurrence (Al-Kindi and Alabri, 2024; Wahba et al., 2024). Despite its computational demand and limited interpretability compared to simpler models like logistic regression, RF remains one of the most reliable and widely used algorithms for flood susceptibility assessment, offering both accuracy and valuable insights through variable importance analysis (Ganjirad and Delavar, 2023; Halder et al., 2024).

3.3 Repeated Hold-Out Method

The Hold-Out method is a commonly used technique for validating machine learning models (Shmueli, 2010). It divides a data set into two parts, one for training and the other for validation. The repeated Hold-Out method is a variant. It overcomes its limitations by averaging model performance over several iterations with different data partitions (Tanner et al., 2019). This provides a more stable estimate of model performance (Monteiro et al., 2016; Pal and Patel, 2020). Here, we used the Repeated Hold-Out method, with 10 random partitions of data, 80% for training and 20% for validation. The two-machine

https://doi.org/10.5194/egusphere-2026-1001
Preprint. Discussion started: 7 April 2026

learning methods are trained on the training set and validated on the test set for each partition, with the performance of each model calculated using the arithmetic mean Equation (1):

$$\bar{P} = \frac{1}{k} \sum_{i=1}^{k} P_i \quad (1)$$

Where P represents the average value of a performance metric, which can be the total accuracy of the model or other metric; k is the number of splits (where k = 10); and Pi is the result of the performance metric of each split.

3.4 Performance Metrics and Evaluation Criteria

The predictive performance of the flood classification models was evaluated using confusion-matrix-based statistical indices by comparing the predicted classes with observed flood occurrences. Four widely adopted metrics were employed: Accuracy (ACC), Precision (PRC), Recall or Sensitivity (SST), and F1-score. These indicators are commonly used in flood susceptibility and spatial modelling studies to quantify classification performance and model reliability (Bouramtane et al., 2022a; Janizadeh et al., 2019). Accuracy (ACC) represents the proportion of correctly classified samples relative to the total number of observations. Precision (PRC) indicates the proportion of correctly predicted flooded areas among all areas classified as flooded, while Recall (SST) measures the ability of the model to correctly identify actual flooded areas. The F1-score combines precision and recall into a single metric, providing a balanced assessment of model performance, particularly in the presence of class imbalance.

The mathematical expressions of the performance metrics are defined as follows:

$$\text{ACC} = \frac{\text{TP}+\text{TN}}{\text{TP}+\text{TN}+\text{FN}+\text{FP}} \quad (2)$$

$$\text{PRC} = \frac{\text{TP}}{\text{TP}+\text{FP}} \quad (3)$$

$$\text{SST} = \frac{\text{TP}}{\text{TP}+\text{FN}} \quad (4)$$

$$\text{F1-score} = \frac{2\times\text{PRC}\times\text{SST}}{\text{PRC}+\text{SST}} \quad (5)$$

Where *TP* denotes true positives, *TN* true negatives, *FP* false positives, and *FN* false negatives.

These metrics were computed for both the training and testing datasets to assess model fitting and generalization capability. Higher values of ACC, PRC, SST, and F1-score indicate better classification performance and improved predictive reliability of the applied models.

3.5 Contribution Analysis of Parameters

The relative contribution of the variables was assessed using the Jackknife test (Efron, 1982), which involves sequentially removing one predictive variable at a time and recalculating the performance of each model to examine the amount of bias or information lost due to the removal of that variable. The sensitivity of each indicator is assessed by the percentage Decrease in overall ACCuracy (DACC).

$$\text{DACCi} = \frac{\text{ACC}_{\text{All}} - \text{ACCi}}{\text{ACC}_{\text{All}}} \times 100 \quad (6)$$

Where ACC All represents the calculated value of the overall accuracy of the model using all parameters. ACCi denotes the ACC value of the model when parameter i is removed from the input dataset, and DACCi is the corresponding percentage decrease in ACC.

https://doi.org/10.5194/egusphere-2026-1001
Preprint. Discussion started: 7 April 2026

4 Results

4.1 Flood Vulnerability Mapping

Using Geographic Information System software, two flood vulnerability maps were produced based on the Random Forest (RF) and Multilayer Perceptron (MLP) algorithms. The resulting flood vulnerability assessment for the Loukkos Basin (Figure 5) classifies the study area into four susceptibility categories: low (0–0.25), medium (0.25–0.5), high (0.5–0.75), and very high (0.75–1). These thresholds represent the probability of a given area being vulnerable to flooding, where values closer to 0 indicate minimal vulnerability and values near 1 indicate maximum vulnerability. Both RF and MLP models

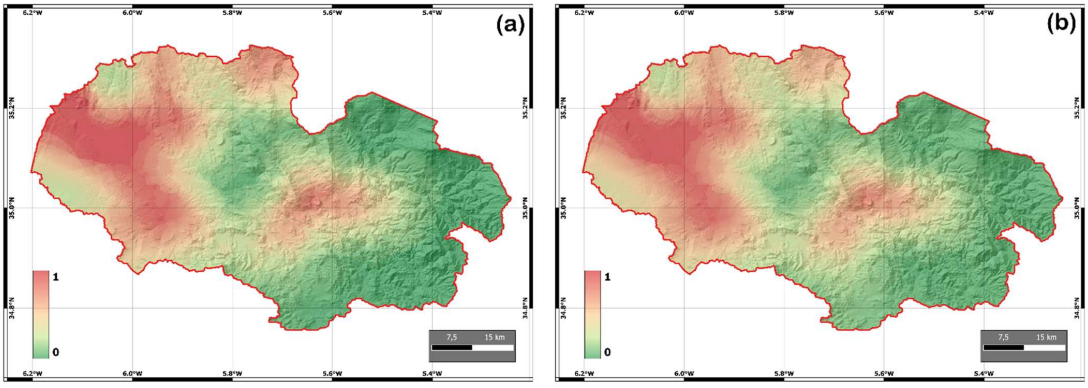

Figure 5: Flood susceptibility maps of the Loukkos Basin generated using (a) the Multilayer Perceptron (MLP) and (b) Random Forest (RF) models.

display comparable spatial patterns of flood susceptibility across the basin. Areas classified as having a very high flood probability correspond closely to the majority of flood points recorded during post flash flood field surveys, while zones of low vulnerability generally encompass non-flooded points demonstrating the robustness and reliability of both models. Although each algorithm captures distinct spatial details, they consistently delineate flood-prone areas concentrated along the Loukkos River, which traverses the basin from east to west, passing through the Oued El Makhazine Dam before discharging into the Atlantic Ocean. The western plains of the study area show particularly high susceptibility, primarily linked to low elevations, high drainage density, and proximity to water channels (Figure 5).

In terms of spatial accuracy and class distribution (Figure 6), both models exhibit a nearly identical allocation across the four vulnerability categories. Specifically, each model indicates that approximately 45% of the study area falls within the low vulnerability class, 24–25% within the medium class, 18–19% within the high class, and 12–13% within the very high vulnerability class. This close correspondence demonstrates the consistency and reliability of the Random Forest and Multilayer Perceptron models in delineating flood-prone areas within the Loukkos Basin.

4.2 Model Validation for Flood Vulnerability Prediction

Tables 1 and 2 present the performance assessment of the Random Forest (RF) and Multilayer Perceptron (MLP) models applied for flood vulnerability prediction. The models were trained and validated using an 80/20 split of the dataset, where 80% of the data were used for model training (Table 1) and the remaining 20% were reserved for independent testing (Table 2). The evaluation relied on four statistical indices (Accuracy, Precision, Recall, and F1 Score) which provide a comprehensive assessment of both classification performance and model generalization capability. As shown in Table 1, both RF and MLP models achieved perfect performance on the training dataset (Accuracy = 1, Precision = 1, Recall = 1, F1 Score = 1).

https://doi.org/10.5194/egusphere-2026-1001
Preprint. Discussion started: 7 April 2026

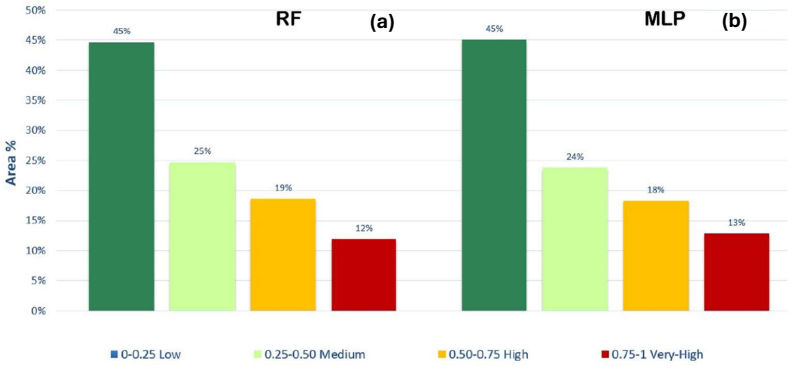

Figure 6: Percentage of area occupied by each vulnerability class determined by the two models over the study area (Loukkos Basin): (a) Random Forest (RF) and (b) Multilayer Perceptron (MLP) models.

These results indicate that the two algorithms successfully learned the patterns in the training data, correctly classifying all samples. However, such perfect performance may also suggest a tendency toward overfitting, highlighting the importance of validating the models on unseen data. The results from the testing dataset (Table 2) provide a more realistic evaluation of model generalization. The MLP model achieved slightly higher predictive performance (Accuracy = 0.909, Precision = 0.909, Recall = 0.909, F1 Score = 0.909) compared to the RF model (Accuracy = 0.864, Precision = 0.833, Recall = 0.909, F1 Score = 0.870). While both models maintained strong predictive capability, the MLP exhibited greater stability and consistency across all statistical indices. The balanced and high values of Precision and F1 Score for the MLP indicate that it is more effective at minimizing false classifications and maintaining reliable predictions for both vulnerable and non-vulnerable areas. Overall, the results confirm that both RF and MLP are powerful classifiers for flood vulnerability mapping, with the MLP showing slightly better generalization performance when applied to the 20% testing dataset. This suggests that MLP may be more robust in capturing complex nonlinear relationships among hydrological and environmental factors influencing flood vulnerability in the study area. The F1 Score was selected as a key indicator of performance in this study because it provides a balanced measure between Precision and Recall, making it particularly suitable for flood vulnerability analysis where the dataset may be imbalanced between vulnerable and non-vulnerable areas. Unlike overall Accuracy, which can be biased by the majority class, the F1 Score reflects the model's true ability to correctly identify both flooded and non-flooded zones. Hence, it offers a more realistic and reliable indicator of predictive capability for flood risk assessment and management applications.

Table 1 Predictive capability of floods models using the training dataset.

Statistical index	RF	MLP
Accuracy	1	1
Precision	1	1
Recall	1	1
F1 Score	1	1

Table 2 Predictive capability of floods models using the testing dataset.

Statistical index	RF	MLP
Accuracy	0.864	0.909

https://doi.org/10.5194/egusphere-2026-1001
Preprint. Discussion started: 7 April 2026

Precision	0.833	0.909
Recall	0.909	0.909
F1 Score	0.870	0.909

4.3 Contribution of Factors to Susceptibility Mapping

The Jackknife-based sensitivity analysis highlights clear variations in the relative influence of conditioning parameters between the RF and MLP models applied in the Loukkos Basin (Figure 7). In the RF model, elevation was identified as the dominant factor, contributing approximately 39% to model performance, followed by slope (17%) and drainage density (13%). These findings indicate that terrain-related variables exert strong control over flood susceptibility in the basin, consistent with its mountainous morphology and steep topographic gradients. Moderate influences were observed for distance from the channel and Topographic Wetness Index (TWI), whereas exposition, curvature, and Topographic Position Index (TPI) had comparatively minor effects. For the MLP model, the distribution of variable importance was more balanced. Elevation remained the most influential factor (around 21%), but TPI, rainfall, and distance from the channel also showed significant contributions, underscoring the importance of both topographic and hydrological drivers in flood occurrence. Factors such as slope, curvature, and drainage density played moderate roles, while TWI and exposition had minimal or negative impacts. Overall, these results emphasize that in the Loukkos Basin, elevation and slope are the primary determinants of flood susceptibility, reflecting the influence of relief on surface runoff generation and flow accumulation. The differences in parameter weighting between RF and MLP also illustrate the distinct learning mechanisms of each algorithm, with RF showing stronger dependence on geomorphological features, while MLP captures a broader combination of topographic and climatic controls.

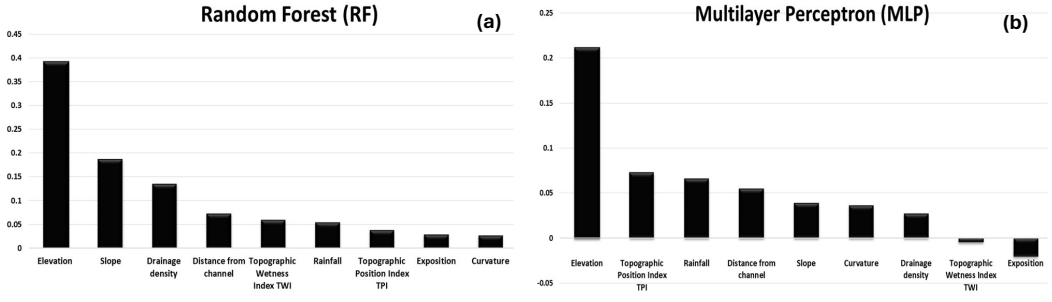

Figure 7. Relative contribution of flood conditioning factors derived from the Jackknife test for (a) the Random Forest (RF) and (b) Multilayer Perceptron (MLP) models in the Loukkos Basin, Northern Morocco.

5 Discussion

The spatial organization of the susceptibility outputs is consistent with a physically plausible flood signal: the highest susceptibility concentrates along the main Loukkos River corridor and the low-relief downstream plains, while upland and higher-gradient zones are generally assigned lower susceptibility. Such patterns are expected in Mediterranean basins where inundation likelihood is strongly controlled by topographic position within the valley–floodplain system and hydraulic connectivity to the drainage network (El Falah et al., 2021; Karrouchi et al., 2016b; El Khalki et al., 2020; Vargas-Yáñez et al., 2010). In the Loukkos setting, the downstream alluvial plain provides the geomorphic "receptor" for floodwater storage: small longitudinal slopes and wide valley-bottom surfaces favor lateral spill and ponding, while channel–floodplain connectivity and the concentration of flow paths toward the main trunk river promote repetitive inundation along the corridor. Similar "river-corridor / downstream-plain" hotspots are widely reported in flood susceptibility mapping across

https://doi.org/10.5194/egusphere-2026-1001
Preprint. Discussion started: 7 April 2026

contrasting basins, where low elevation and gentle slopes promote floodplain expansion and longer water residence times (Bouramtane et al., 2020; Hitouri et al., 2024; Meliho et al., 2025).

Despite algorithmic differences, both approaches produce broadly consistent spatial patterns, and the class-area distributions indicate a structured susceptibility field rather than diffuse hazard (≈45% low; ≈24–25% medium; ≈18–19% high; ≈12–13% very high). This agreement matters because it implies that the mapped susceptibility is not simply an artefact of one learner but reflects stable relationships between flood occurrence and the predictor space. In other words, the models converge toward similar "hotspot geometry" because the conditioning factors encode coherent floodplain controls (valley-bottom position, proximity to drainage, and hydrologic convergence) rather than idiosyncratic patterns tied to a single training run. This convergence is also useful from an applied standpoint: it provides a basic robustness check that is often missing when only one algorithm is reported, and it allows planners to interpret overlapping high-susceptibility zones as more reliable screening targets than isolated hotspots produced by one method alone.

At the same time, differences in class allocation and performance indicate that the two models encode the predictor–flood relationship with different "decision surfaces". RF offers strong predictive skill and a transparent ranking of factor influence (Abbasi et al., 2023; Al-Aizari et al., 2024; Ganjirad and Delavar, 2023; Lee et al., 2017; Tepetidis et al., 2025), whereas MLP can represent more complex non-linear interactions among conditioning factors, which is often advantageous when flood occurrence emerges from multi-factor coupling rather than separable thresholds (Ahmadlou et al., 2021; Andaryani et al., 2021; Janizadeh et al., 2019; Motta et al., 2021). In our results, MLP shows higher overall test performance (accuracy and F1), while RF exhibits lower precision consistent with a tendency to label more locations as flood-prone (i.e., a more conservative susceptibility delineation). This trade-off is common in susceptibility mapping and has practical implications: a higher-recall/lower-precision model may be preferred for screening and precautionary planning (minimizing missed hotspots), whereas a higher-precision model may be preferable when mitigation resources are tightly limited, interventions must be targeted, and false positives carry high opportunity costs.

The predictor contribution analysis highlights terrain as the dominant control, especially in RF where elevation and slope explain a large fraction of model influence. This is consistent with a broad literature showing that morphometric predictors often dominate basin-scale susceptibility because they capture floodplain position, local relief, and flow convergence at the scale at which susceptibility maps are typically produced (Bouramtane et al., 2021; Hitouri et al., 2024; Mekkaoui et al., 2025; Motta et al., 2021). Elevation is a first-order proxy for valley-bottom location and the local base-level context that governs where water can accumulate, while slope separates flat floodplain surfaces from better-drained terraces and hillslopes where water routing is rapid and inundation is less persistent. Additional morphometric descriptors (e.g., drainage density, curvature-related proxies, and topographic indices) act as integrative measures of flow concentration and convergence, which is why they often emerge as important even when precipitation information is present.

In contrast, the more balanced importance distribution in MLP, where rainfall and distance-to-channel become more prominent, suggests that the neural network is exploiting interaction effects (e.g., "low elevation × proximity × higher rainfall"), rather than relying on a single dominant threshold. This is plausible because rainfall variability and antecedent wetness proxies can provide discriminating power within broadly low-relief regions where terrain alone may not separate frequently inundated micro-domains from adjacent but less connected surfaces (Motta et al., 2021). Importantly, the relative role of rainfall is known to vary strongly with climate regime and event type: studies in monsoon-influenced or El Niño-affected regions often report greater leverage of rainfall or moisture proxies because extremes dominate flood generation (Abijith et al., 2025; Badillo-Rivera et al., 2025). In Mediterranean contexts, storm sequencing and basin wetness memory can be critical, meaning that rainfall products may help represent event intensity and persistence even when they remain simplified relative to the true spatiotemporal dynamics of storms and runoff response.

Our use of repeated hold-out validation provides a defensible and transparent estimate of out-of-sample performance because the models are evaluated on data not used for fitting, and repetition reduces sensitivity to one particular split (Bouramtane et

https://doi.org/10.5194/egusphere-2026-1001
Preprint. Discussion started: 7 April 2026

al., 2022a; Monteiro et al., 2016). The resulting test metrics (MLP accuracy/F1 ≈0.91; RF accuracy ≈0.86, F1 ≈0.87) indicate that susceptibility patterns are not merely descriptive, but retain predictive value when confronted with withheld observations. This is important because it supports the interpretation of the maps as probability-like indicators of flood predisposition rather than as purely explanatory overlays of the training inventory.

However, as in most susceptibility studies, a key caveat is that random Hold-Out can overestimate generalization when samples are spatially clustered (i.e., training and test points share similar predictor neighbourhoods). A spatially blocked evaluation would be a stronger stress test for map transferability, particularly if the susceptibility product is intended for zoning decisions beyond the densest inventory areas. This limitation is widely recognized in the ML-based flood susceptibility literature and motivates reporting validation choices clearly alongside intended use-cases (Bouramtane et al., 2022b; Pourzangbar et al., 2025). In practice, blocked cross-validation would help quantify whether model skill persists when applied to predictor combinations that are not "nearby cousins" of the training samples, which is the relevant question when maps are used to support basin-wide screening and prioritization.

Within Morocco, our results align with multiple recent applications showing that ML-based susceptibility mapping can delineate flood-prone zones effectively in data-limited contexts, with downstream plains and channel-adjacent areas emerging consistently as hotspots (Hitouri et al., 2024; Meliho et al., 2025; Sellami et al., 2022). Urban-scale studies in Morocco further demonstrate that RF and related ML methods can perform well for hazard/susceptibility mapping when predictor layers are carefully assembled, though performance and the "dominant predictors" may shift with scale, urban fabric, and inventory definition (El baida et al., 2024; Boushaba et al., 2024). This scale dependence is not trivial: basin-scale susceptibility layers are well suited to flagging floodplain predisposition and guiding where more detailed analyses should focus, but neighborhood-scale flood impacts can be strongly modulated by drainage infrastructure, local micro-topography, and flow obstructions that are not necessarily resolved by regional predictors.

Across contrasting environments, the relative ranking of RF vs. neural network approaches is mixed: some basins report RF or tree-ensembles as best performers, while others show comparable or superior results for neural networks depending on sample size, predictor collinearity, and how floods are inventoried (Abijith et al., 2025; Pourzangbar et al., 2025). Our finding that MLP slightly outperforms RF is therefore credible and fits the broader evidence that no single algorithm dominates universally; instead, performance hinges on how well model structure matches the underlying data-generation process and the representativeness of the inventory. In settings where flood occurrence reflects coupled controls and non-linear thresholds (for example, lowland connectivity interacting with event persistence), MLP-like models can benefit from their capacity to encode interactions without explicitly predefining them.

A key strength of our approach is the convergence of two independent ML models toward consistent susceptibility hotspots, paired with explicit out-of-sample testing. The susceptibility maps therefore provide a practical basis for risk screening, prioritization of detailed hydraulic studies, and guiding land-use constraints in the most susceptible plains and river-adjacent zones (El Khalki et al., 2020). In addition, the January–February 2026 flood episode (Figure 8) offers a qualitative "post-study" consistency check: the broad distribution of inundation visible in satellite imagery and documented impacts appears to overlap the same low-lying floodplain sectors and channel-adjacent corridors that our models classify as high to very high susceptibility. While this does not replace a formal independent validation dataset (with consistent inventory rules and sampling), it strengthens confidence that the mapped hotspots reflect persistent geomorphic predisposition rather than a one-off pattern tied to the 2022 event used for training.

The 2026 episode also highlights that flood severity in the lower Loukkos should be interpreted through the lens of compound flooding, where fluvial discharge interacts with coastal water levels and nearshore conditions. In estuarine settings, elevated sea level during high tide can reduce the downstream hydraulic gradient at the river mouth, producing a backwater response that slows drainage to the ocean and can raise upstream water levels across low-relief floodplains (Hoitink and Jay, 2016; Moftakhari et al., 2019; Harrison et al., 2022). When high river discharge persists over several tidal

https://doi.org/10.5194/egusphere-2026-1001
Preprint. Discussion started: 7 April 2026

cycles, the interaction can translate into longer inundation duration and delayed recession even after rainfall intensity weakens, particularly in wide coastal plains where small stage differences matter for overbank extent (Familkhalili et al., 2022; Harrison et al., 2022). This interpretation is consistent with the broader compound-event literature showing that co-occurring high sea levels and extreme precipitation/discharge can amplify flood hazard relative to either driver alone (Wahl et al., 2015; Ward et al., 2018; Bevacqua et al., 2019; Green et al., 2025). For the Loukkos mouth near Larache, where coastal forcing can be further influenced by swell and storm conditions, local reporting during the 2026 crisis explicitly invoked the role of high tide/rough sea states in worsening drainage conditions (Kharroubi, 2026). Taken together, these lines of evidence support treating the lower Loukkos as a system where flood impacts may be disproportionately large when fluvial peaks coincide with unfavorable coastal boundary conditions.

From a susceptibility-mapping perspective, the tide/backwater mechanism clarifies both the value and the limits of static ML products. On one hand, susceptibility maps are expected to perform well at identifying where floodwaters preferentially spread because topography and proximity to drainage encode persistent predisposition; this is consistent with the agreement between modeled hotspots and observed inundation corridors. On the other hand, event-scale amplification from time-varying boundary conditions (tide, storm surge, wave setup, and potentially operational releases) is not fully represented by static predictors, meaning that susceptibility classes should not be interpreted as deterministic forecasts of event magnitude or duration. This limitation is widely recognized in the compound flooding literature, which emphasizes the need for modeling frameworks that couple catchment-to-coast drivers when the objective is to quantify extreme water levels or impact severity rather than predisposition alone (Wahl et al., 2015; Moftakhari et al., 2019; Green et al., 2025). A natural extension for the Loukkos system would therefore be to integrate susceptibility screening with event-time information (river stage, rainfall forecasts, dam operations, and tidal predictions) in order to better represent compound forcing when prioritizing emergency actions.

The principal limitations are those typical of ML susceptibility products: dependence on the quality/representativeness of the flood inventory, the static nature of many predictors, and potential optimism under random validation when spatial autocorrelation is present. Because our inventory is derived from Sentinel-1 change detection, mapped flood extents can be influenced by threshold choices, land cover, and backscatter variability; these sensitivities are well documented in comparative assessments of Sentinel-1 flood mapping algorithms (Abbasi et al., 2023; Isundwa et al., 2025; Tazmul Islam and Meng, 2022; Tupas et al., 2023; Zhao et al., 2024). In agricultural floodplains, an additional challenge is the partial

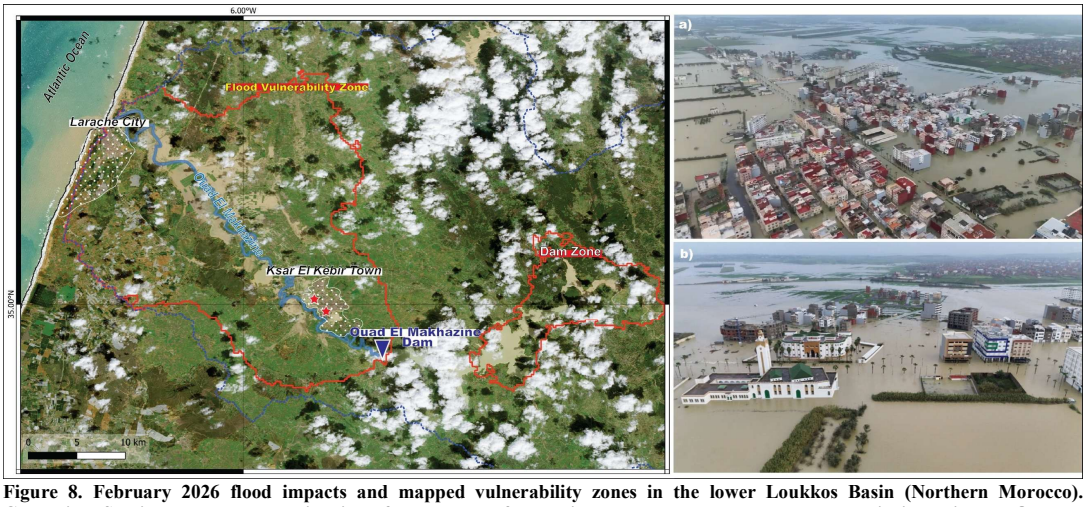

Figure 8. February 2026 flood impacts and mapped vulnerability zones in the lower Loukkos Basin (Northern Morocco). Copernicus Sentinel true-color satellite view of the Loukkos floodplain between Larache and Ksar El Kebir, including the Oued El Makhazine River and Dam locations. Red outlines delimit the main flood-vulnerability zone analyzed in this study. The blue dashed line indicates the basin boundary. (a and b) illustrative photographs showing extensive floods of urban and peri-urban areas during the January–February 2026 flood episode.

https://doi.org/10.5194/egusphere-2026-1001
Preprint. Discussion started: 7 April 2026

ambiguity between shallow inundation and saturated soils or vegetation-related backscatter changes, which can introduce omission/commission errors depending on acquisition timing and land-surface conditions (DeVries et al., 2020; Wagner et al., 2026). These points motivate expanding the inventory across multiple events and seasons and, where possible, cross-checking SAR-derived flood masks with optical imagery and ground reports to reduce sensitivity to single-date thresholds.

From an applied perspective, the most direct implication is that the very high susceptibility class (≈12–13% of the basin) can be treated as a priority zone for floodplain regulation, infrastructure siting constraints, and emergency planning. Meanwhile, the medium and high classes (together ≈42–44%) can inform staged mitigation—e.g., targeted drainage upgrades, river corridor setbacks, and monitoring—recognizing that susceptibility is a probability-like tendency rather than a deterministic forecast. In the lower Loukkos, the compound-flooding discussion further implies that preparedness should not rely on rainfall/discharge alone but should also consider the timing of peak flows relative to the tidal cycle and coastal conditions, because unfavorable sea-level boundary states can delay drainage and prolong impacts in the coastal floodplain (Hoitink and Jay, 2016; Ward et al., 2018; Familkhalili et al., 2022; Green et al., 2025). Operationally, this supports a tiered approach in which susceptibility maps guide where to prioritize, while real-time hydro-meteorological and coastal monitoring guides when the highest-impact conditions are likely to emerge.

6 Conclusion

This study developed a flood susceptibility mapping framework for the Loukkos Basin (northern Morocco) that is explicitly anchored in observed inundation and designed for reproducible model evaluation. By combining a Sentinel-1 SAR–derived flood inventory with high-resolution geomorphometric predictors and rainfall information, the approach provides a practical pathway to characterize flood-prone zones in a context where long discharge records and detailed hydraulic datasets are often limited.

The susceptibility maps produced by the RF and MLP models consistently highlighted the basin's most flood-exposed environments: low-elevation areas with high hydraulic connectivity to the river network, particularly along the main channels, near confluences, and across broad floodplain sectors. These patterns align with the physical expectation that inundation likelihood increases where topographic gradients are low, flow accumulation is high, and distance to channels is small—conditions that favor overflow, backwater effects, and longer water residence times during extreme rainfall episodes. Importantly, the repeated hold-out validation strategy provided a more stable estimate of generalization skill than a single train–test split, strengthening confidence that model performance reflects transferable relationships rather than partition-specific results.

Beyond predictive performance, the study emphasizes interpretability as a requirement for risk-informed decision making. The jackknife-style factor analysis (expressed as performance decrease when removing one predictor at a time) helps identify which controls are most influential in the Loukkos setting and clarifies why specific zones repeatedly emerge as susceptibility hotspots. This diagnostic is particularly valuable for communication with planners and water managers, because it links mapped outcomes to measurable basin characteristics rather than treating the model as a black box.

From an applied perspective, the outputs of this work are directly relevant to flood risk reduction in northern Morocco. The susceptibility classes can support: (i) preliminary zoning for land-use regulation and the protection of floodplain functions; (ii) prioritization of field surveys and hydraulic modeling in the most susceptible corridors; (iii) identification of critical infrastructure and agricultural sectors that require targeted protection; and (iv) screening of candidate sites for mitigation measures such as improved drainage, retention enhancement, and nature-based solutions. While susceptibility mapping does not replace hydraulic modeling for design-level flood depths and velocities, it provides a defensible basin-scale foundation for deciding where detailed investigations and investments should be concentrated.

https://doi.org/10.5194/egusphere-2026-1001
Preprint. Discussion started: 7 April 2026

A post-study validation by the 2026 flood crisis. Shortly after completing this work, the lower Loukkos basin experienced a major flood emergency from late January to mid-February 2026, following weeks of heavy rainfall on saturated catchments combined with controlled releases from the Oued El Makhazine dam. Preventive evacuations exceeded 150,000 people, with Larache province among the most impacted, and Ksar El Kebir placed under maximum flood alert during peak flooding. This event provides an external reality check for our susceptibility outputs: the inundated zones visible in the Sentinel image acquired on 14 February 2026 (Figure 8) concentrate within the same low-lying floodplain sectors and the high/very-high susceptibility corridors highlighted by our best-performing models (RF/MLP). Beyond methodological performance, this confirms the operational value of the proposed framework for preparedness, rapid prioritization of exposed rural areas, and planning of mitigation measures in the Loukkos floodplain.

Several limitations also define priorities for future work. First, an event-based inventory—although observationally strong—captures a particular hydro meteorological realization; expanding the inventory to multiple flood events and seasons would improve robustness and reduce sensitivity to event-specific conditions. Second, SAR flood delineation can be affected by vegetation cover, rough water surfaces, complex urban backscatter, and mixed pixels near the channel margins; systematic uncertainty characterization and multi-sensor fusion (e.g., combining SAR with cloud-free optical windows and field evidence) would further strengthen inventory reliability. Third, susceptibility predictors were treated as largely static; integrating land-use dynamics, soil moisture proxies, and improved rainfall extremes (including local gauge adjustment where available) would better represent triggering processes and spatial forcing gradients. Finally, coupling susceptibility outputs with hydraulic simulations for selected reaches could translate susceptibility zones into flood depth/velocity products for engineering design and emergency planning. Overall, the study provides an event-informed, interpretable, and reproducible flood susceptibility framework for the Loukkos Basin. The combined use of SAR-derived inundation evidence, comparative ML modeling, repeated validation, and predictor-contribution diagnostics offers a practical template that can be extended to other Moroccan basins facing similar exposure growth and extreme-rainfall risk.

Author contributions

O M designed the study, defined the methodology, and led the overall research framework, analyzed the data, interpreted the results, and prepared the original manuscript draft. M M contributed to data analysis and revised and corrected the manuscript draft. T B contributed to data analysis and supported the interpretation of the results. H A contributed to data analysis, modeling, and writing of specific sections of the manuscript. All authors reviewed the manuscript and approved the final version.

Competing interests

The authors declare that they have no competing interests.

Acknowledgements

Besides the author's statement of gratitude to and recognition of the people and institutions that helped the author's research and writing, authors are also asked to include relevant research infrastructure they have benefitted from during their research, where research was conducted or data/resources were used. Examples are Field Stations and Marine Laboratories (FSMLs).

Financial support

The authors received no specific funding for this work.

https://doi.org/10.5194/egusphere-2026-1001
Preprint. Discussion started: 7 April 2026

References

Abbasi, M., Shah-hosseini, R., and Forest, R.: Sentinel-1 Polarization Comparison for Flood Segmentation Using Deep Learning † and a Feature Pyramid Network (FPN), both based on the E ffi cientNet-B7 backbone . The evaluated the performance of the models using the Sentinel-1 images . Using several m, Proc. MDPI, 1–8, 2023.

ABHL Agence du Bassin Hydraulique du Loukkos: RAPPORT DES RESULTATS, 2016.

Abijith, D., Saravanan, S., Parthasarathy, K. S. S., Reddy, N. M., Niraimathi, J., Bindajam, A. A., Mallick, J., Alharbi, M. M., and Abdo, H. G.: Assessing the impact of climate and land use change on flood vulnerability: a machine learning approach in coastal region of Tamil Nadu, India, Geosci. Lett., 12, 1, 2025.

Acharki, S., Taia, S., Arjdal, Y., and Hack, J.: Hydrological modeling of spatial and temporal variations in streamflow due to multiple climate change scenarios in northwestern Morocco, Clim. Serv., 30, 100388, https://doi.org/10.1016/j.cliser.2023.100388, 2023.

Agharroud, K., Puddu, M., Ivčević, A., Satta, A., Kolker, A. S., and Snoussi, M.: Climate risk assessment of the Tangier-Tetouan-Al Hoceima coastal Region (Morocco), Front. Mar. Sci., 10, 1176350, 2023.

Ahmadlou, M., Al-Fugara, A., Al-Shabeeb, A. R., Arora, A., Al-Adamat, R., Pham, Q. B., Al-Ansari, N., Linh, N. T. T., and Sajedi, H.: Flood susceptibility mapping and assessment using a novel deep learning model combining multilayer perceptron and autoencoder neural networks, J. Flood Risk Manag., 14, e12683, 2021.

Al-Aizari, A. R., Alzahrani, H., Althuwaynee, O. F., Al-Masnay, Y. A., Ullah, K., Park, H.-J., Al-Areeq, N. M., Rahman, M., Hazaea, B. Y., and Liu, X.: Uncertainty reduction in Flood susceptibility mapping using Random Forest and eXtreme Gradient Boosting algorithms in two Tropical Desert cities, Shibam and Marib, Yemen, Remote Sens., 16, 336, 2024.

AL-Hussein, A. A. M., Khan, S., Ncibi, K., Hamdi, N., and Hamed, Y.: Flood Analysis Using HEC-RAS and HEC-HMS: A Case Study of Khazir River (Middle East—Northern Iraq), https://doi.org/10.3390/w14223779, 2022.

Al-Kindi, K. M. and Alabri, Z.: Investigating the role of the key conditioning factors in flood susceptibility mapping through machine learning approaches, Earth Syst. Environ., 8, 63–81, 2024.

Alami, A. El and Jilali, A.: A Three-Dimensional Geological Model of the R'Mel Aquifer, Northwestern Morocco, Iraqi Geol. J., 56, 14–28, https://doi.org/10.46717/igj.56.1D.2ms-2023-4-11, 2023.

Alexander, M., Viavattene, C., Faulkner, H., and Priest, S.: A GIS-based flood risk assessment tool: supporting flood incident management at the local scale, Flood Hazard Res. Centre, Middlesex Univ. London, 2011.

Andaryani, S., Nourani, V., Haghighi, A. T., and Keesstra, S.: Integration of hard and soft supervised machine learning for flood susceptibility mapping, J. Environ. Manage., 291, 112731, 2021.

Asghar Rostami, A., Taghi Sattari, M., Apaydin, H., and Milewski, A.: Modeling Flood Susceptibility Utilizing Advanced Ensemble Machine Learning Techniques in the Marand Plain, https://doi.org/10.3390/geosciences15030110, 2025.

Azouagh, A., Bardai, R., Hilal, I., and Messari, J.: Integration of GIS and HEC-RAS in Floods Modeling of Martil River (Northern Morocco), Eur. Sci. J., 14, https://doi.org/10.19044/esj.2018.v14n12p130, 2018.

Badillo-Rivera, E., Santiago, R., Poma, I., Chavez, T., Arroyo-Paz, A., Aucahuasi-Almidon, A., Hinostroza, E., Segura, E., Eyzaguirre, L., León, H., and Virú-Vásquez, P.: Flood susceptibility mapping in El Niño Phenomenom integrating multitemporal radar analysis, GIS and machine learning techniques, Piura river basin, Peru, Front. Environ. Sci., 13, 1–20, https://doi.org/10.3389/fenvs.2025.1672107, 2025.

El baida, M., Boushaba, F., Chourak, M., Hosni, M., and Sabar, H.: Classification machine learning models for urban flood hazard mapping: case study of Zaio, NE Morocco, Nat. Hazards, 120, 10013–10041, 2024.

Benchbani, I., Sebari, K., and Zemzami, M.: Integrated water resources management in the Loukkos basin (Morocco): an approach to improve resilience under climate change impact, in: E3S Web of Conferences, 3024, 2022.

Bevacqua, E., Maraun, D., Vousdoukas, M. I., Voukouvalas, E., Vrac, M., Mentaschi, L., and Widmann, M.: Higher probability of compound flooding from precipitation and storm surge in Europe under anthropogenic climate change, Sci.

https://doi.org/10.5194/egusphere-2026-1001
Preprint. Discussion started: 7 April 2026

Adv., 5, eaaw5531, https://doi.org/10.1126/sciadv.aaw5531, 2019.

Bouramtane, T., Yameogo, S., Touzani, M., Janati, M. H. El, Ouardi, J., Kacimi, I., and Vallès, V.: Statistical approach of factors controlling drainage network patterns in arid areas . Application to the Eastern Anti Atlas (Morocco) HAL Id : hal-02389502, https://doi.org/10.1016/j.jafrearsci.2019.103707, 2020.

Bouramtane, T., Kacimi, I., Bouramtane, K., Aziz, M., Abraham, S., Omari, K., Valles, V., Leblanc, M., Kassou, N., El Beqqali, O., Bahaj, T., Morarech, M., Yameogo, S., and Barbiero, L.: Multivariate Analysis and Machine Learning Approach for Mapping the Variability and Vulnerability of Urban Flooding: The Case of Tangier City, Morocco, https://doi.org/10.3390/hydrology8040182, 2021.

Bouramtane, T., Hilal, H., Rezende-Filho, A. T., Bouramtane, K., Barbiero, L., Abraham, S., Valles, V., Kacimi, I., Sanhaji, H., and Torres-Rondon, L.: Mapping gully erosion variability and susceptibility using remote sensing, multivariate statistical analysis, and machine learning in South Mato Grosso, Brazil, Geosciences, 12, 235, 2022a.

Bouramtane, T., Hilal, H., Rezende-filho, A. T., Bouramtane, K., and Barbiero, L.: Mapping Gully Erosion Variability and Susceptibility Using Remote Sensing , Multivariate Statistical Analysis , and Machine Learning in South Mato Grosso , Mapping Gully Erosion Variability and Susceptibility Using Remote Sensing , Multivariate Statistica, https://doi.org/10.3390/geosciences12060235, 2022b.

Boushaba, F., Chourak, M., Hosni, M., Sabar, H., and Zahaf, T.: Flood risk decomposed: Optimized machine learning hazard mapping and multi-criteria vulnerability analysis in the city of Zaio, Morocco, J. African Earth Sci., 220, 105431, 2024.

Breiman, L.: Random Forests, Mach. Learn., 45, 5–32, https://doi.org/10.1023/A:1010933404324, 2001.

Cao, H., Zhang, H., Wang, C., and Zhang, B.: Operational flood detection using Sentinel-1 SAR data over large areas, Water (Switzerland), 11, https://doi.org/10.3390/w11040786, 2019.

Chan, K. Y., Abu-Salih, B., Qaddoura, R., Al-Zoubi, A. M., Palade, V., Pham, D.-S., Ser, J. Del, and Muhammad, K.: Deep neural networks in the cloud: Review, applications, challenges and research directions, Neurocomputing, 545, 126327, https://doi.org/https://doi.org/10.1016/j.neucom.2023.126327, 2023.

Chauhan, S., Dongol, R., and Chauhan, R.: Evaluation of economic loss of urban road flooding: A case of Kathmandu Metropolitan City, Environ. Challenges, 13, 100773, https://doi.org/https://doi.org/10.1016/j.envc.2023.100773, 2023.

Chen, J.-F., Do, Q. H., and Hsieh, H.-N.: Training Artificial Neural Networks by a Hybrid PSO-CS Algorithm, https://doi.org/10.3390/a8020292, 2015.

Choubin, B., Borji, M., Mosavi, A., Sajedi-Hosseini, F., Singh, V. P., and Shamshirband, S.: Snow avalanche hazard prediction using machine learning methods, J. Hydrol., 577, 123929, 2019.

DeVries, B., Huang, C., Armston, J., Huang, W., Jones, J. W., and Lang, M. W.: Rapid and robust monitoring of flood events using Sentinel-1 and Landsat data on the Google Earth Engine, Remote Sens. Environ., 240, 111664, https://doi.org/10.1016/j.rse.2020.111664, 2020.

Efron, B.: The jackknife, the bootstrap and other resampling plans, SIAM, 1982.

El Falah, S., Dakki, M., and Mansouri, I.: Mapping analysis of the wetland loss in loukkos (Morocco) under agricultural managements, Bulg. J. Agric. Sci., 27, 186–193, 2021.

Familkhalili, R., Talke, S. A., and Jay, D. A.: Compound flooding in convergent estuaries: insights from an analytical model, Ocean Sci., 18, 1203–1220, https://doi.org/10.5194/os-18-1203-2022, 2022.

Fawcett, T.: An introduction to ROC analysis, Pattern Recognit. Lett., 27, 861–874, 2006.

Feizbahr, M., Brake, N., Arbabkhah, H., Hariri Asli, H., and Woods, K.: Flood Susceptibility Mapping Using Machine Learning and Geospatial-Sentinel-1 SAR Integration for Enhanced Early Warning Systems, Remote Sens., 17, 1–30, https://doi.org/10.3390/rs17203471, 2025.

Ganjirad, M. and Delavar, M. R.: FLOOD RISK MAPPING USING RANDOM FOREST AND SUPPORT VECTOR

https://doi.org/10.5194/egusphere-2026-1001
Preprint. Discussion started: 7 April 2026

MACHINE, ISPRS Ann. Photogramm. Remote Sens. Spat. Inf. Sci., X-4/W1-202, 201–208, https://doi.org/10.5194/isprs-annals-X-4-W1-2022-201-2023, 2023.

Green, J., Haigh, I. D., Quinn, N., Neal, J., Wahl, T., Wood, M., Eilander, D., de Ruiter, M., Ward, P., and Camus, P.: Review article: A comprehensive review of compound flooding literature with a focus on coastal and estuarine regions, Nat. Hazards Earth Syst. Sci., 25, 747–816, https://doi.org/10.5194/nhess-25-747-2025, 2025.

Halder, K., Ghosh, A., Srivastava, A. K., Pal, S. C., Chatterjee, U., Bisai, D., Ewert, F., Gaiser, T., Islam, A. R. M. T., and Alam, E.: SAR-driven flood inventory and multi-factor ensemble susceptibility modelling using machine learning frameworks, Geomatics, Nat. Hazards Risk, 15, 2409202, 2024.

Handayani, W., Chigbu, U. E., Rudiarto, I., and Putri, I. H.: Urbanization and Increasing Flood Risk in the Northern Coast of Central Java—Indonesia: An Assessment towards Better Land Use Policy and Flood Management, https://doi.org/10.3390/land9100343, 2020.

Haribabu, S., Gupta, G. S., Kumar, P. N., and Rajendran, P. S.: Prediction of flood by rainf all using MLP classifier of neural network model, in: 2021 6th international conference on communication and electronics systems (ICCES), 1360–1365, 2021.

Harrison, L. M., Coulthard, T. J., Robins, P. E., and Lewis, M. J.: Sensitivity of estuaries to compound flooding, Estuaries Coasts, 45, 1250–1269, https://doi.org/10.1007/s12237-021-00996-1, 2022.

Hitouri, S., Mohajane, M., Lahsaini, M., Ali, S. A., Setargie, T. A., Tripathi, G., Antonio, P. D., Singh, S. K., and Varasano, A.: Flood Susceptibility Mapping Using SAR Data and Machine Learning Algorithms in a Small Watershed in Northwestern Morocco, 2024.

Hossain, M. K. and Meng, Q.: A fine-scale spatial analytics of the assessment and mapping of buildings and population at different risk levels of urban flood, Land use policy, 99, 104829, 2020a.

Hossain, M. K. and Meng, Q.: Land Use Policy A fi ne-scale spatial analytics of the assessment and mapping of buildings and population at di ff erent risk levels of urban fl ood, Land use policy, 99, 104829, https://doi.org/10.1016/j.landusepol.2020.104829, 2020b.

Hoitink, A. J. F., & Jay, D. A. (2016). Tidal river dynamics: Implications for deltas. Reviews of Geophysics, 54(1), 240–272. https://doi.org/10.1002/2015RG000507

Isundwa, F., Armando, M., Berardi, A., Bovolo, C., Hunter, P., Neil, C., Silva-Perez, C., and Silva, T.: Optimizing Change Detection Methods for Flood Mapping Using Polarimetric SAR, IEEE J. Sel. Top. Appl. Earth Obs. Remote Sens., PP, 1–14, https://doi.org/10.1109/JSTARS.2025.3628450, 2025.

Ivčević, A., Bertoldo, R., Mazurek, H., Siame, L., Guignard, S., Moussa, A. Ben, and Bellier, O.: Local risk awareness and precautionary behaviour in a multi-hazard region of North Morocco, Int. J. Disaster Risk Reduct., 50, 101724, 2020.

Janizadeh, S., Avand, M., Jaafari, A., Phong, T. V, Bayat, M., Ahmadisharaf, E., Prakash, I., Pham, B. T., and Lee, S.: Prediction Success of Machine Learning Methods for Flash Flood Susceptibility Mapping in the Tafresh Watershed, Iran, https://doi.org/10.3390/su11195426, 2019.

Karrouchi, M., Touhami, M. O., Oujidi, M., and Chourak, M.: Cartographie des zones à risque d ' inondation dans la région Tanger-Tétouan : Cas du bassin versant de Martil (Nord du Maroc) [Mapping of flooding risk areas in the Tangier-Tetouan region : Case of Martil Watershed (Northern Morocco)], 14, 1019–1035, 2016a.

Karrouchi, M., Touhami, M. O., Oujidi, M., and Chourak, M.: Mapping of flooding risk areas in the Tangier-Tetouan region: Case of Martil Watershed (Northern Morocco), Int. J. Innov. Appl. Stud., 14, 1019–1035, 2016b.

Kharroubi, H.: À Ksar El Kébir, 54.000 habitants évacués: pourquoi la ville est sous les eaux et à quels risques faut-il s'attendre?, Le360, 3 February 2026, https://fr.le360.ma/societe/a-ksar-el-kebir-54000-habitants-evacues-pourquoi-la-ville-est-sous-les-eaux-et-a-quels-risques-faut_KLZUCZL3GVHMLCC5QUQEC6S44Q/, 2026.

El Khalki, E. M., Tramblay, Y., Massari, C., Brocca, L., Simonneaux, V., Gascoin, S., and Saidi, M. E. M.: Challenges in

https://doi.org/10.5194/egusphere-2026-1001
Preprint. Discussion started: 7 April 2026

flood modeling over data-scarce regions: how to exploit globally available soil moisture products to estimate antecedent soil wetness conditions in Morocco, Nat. Hazards Earth Syst. Sci., 20, 2591–2607, https://doi.org/10.5194/nhess-20-2591-2020, 2020.

Kim, S. Y., Lee, Y., and Park, S. E.: On Flood Detection Using Dual-Polarimetric SAR Observation, Remote Sens., 17, 1–19, https://doi.org/10.3390/rs17111931, 2025.

Kohavi, R.: A study of cross-validation and bootstrap for accuracy estimation and model selection, in: Ijcai, 1137–1145, 1995.

Lee, S., Kim, J.-C., Jung, H.-S., Lee, M. J., and Lee, S.: Spatial prediction of flood susceptibility using random-forest and boosted-tree models in Seoul metropolitan city, Korea, Geomatics, Nat. Hazards Risk, 8, 1185–1203, 2017.

Martín-Martín, M., Guerrera, F., Hlila, R., Maaté, A., Maaté, S., Tramontana, M., Serrano, F., Cañaveras, J. C., Alcalá, F. J., and Paton, D.: Tectono-sedimentary cenozoic evolution of the El habt and ouezzane tectonic units (external rif, Morocco), Geosciences, 10, 487, 2020.

Masson-Delmotte, V., Zhai, P., Pirani, A., Connors, S. L., Péan, C., Berger, S., Caud, N., Chen, Y., Goldfarb, L., and Gomis, M. I.: Climate change 2021: the physical science basis, Contrib. Work. Gr. I to sixth Assess. Rep. Intergov. panel Clim. Chang., 2, 2391, 2021.

Mekkaoui, O., Morarech, M., Bouramtane, T., Barbiero, L., Hamidi, M., Akka, H., and Rengasamy, R. P. M.: Unveiling Urban Flood Vulnerability: A Machine Learning Approach for Mapping High Risk Zones in Tetouan City, Northern Morocco, Urban Sci., 9, https://doi.org/10.3390/urbansci9030070, 2025.

Meliho, M., Khattabi, A., Driss, Z., and Orlando, C. A.: Spatial prediction of flood-susceptible zones in the Ourika watershed of Morocco using machine learning algorithms, Appl. Comput. Informatics, 21, 317–329, 2025.

Miller, J. D. and Hutchins, M.: The impacts of urbanisation and climate change on urban flooding and urban water quality: A review of the evidence concerning the United Kingdom, J. Hydrol. Reg. Stud., 12, 345–362, https://doi.org/https://doi.org/10.1016/j.ejrh.2017.06.006, 2017.

Ministère de l'Équipement et de L'eau: Maroc: Etat du climat en 2023, Roy. du Maroc- Ministère l'Équipement l'eau-Ministère l'Équipement l'eau, 167–186, 2023.

El Moçayd, N., Kang, S., and Eltahir, E. A. B.: Climate change impacts on the Water Highway project in Morocco, Hydrol. Earth Syst. Sci., 24, 1467–1483, https://doi.org/10.5194/hess-24-1467-2020, 2020.

Moftakhari, H., Schubert, J. E., AghaKouchak, A., Matthew, R. A., and Sanders, B. F.: Linking statistical and hydrodynamic modeling for compound flood hazard assessment in tidal channels and estuaries, Adv. Water Resour., 128, 28–38, https://doi.org/10.1016/j.advwatres.2019.04.009, 2019.

Monika, G. and Berezowski, T.: A Physics-Guided Neural Network for Flooding Area Detection Using SAR Imagery and Local River Gauge Observations, IEEE J. Sel. Top. Appl. Earth Obs. Remote Sens., PP, 1–15, https://doi.org/10.1109/JSTARS.2025.3561926, 2025.

Monteiro, J. M., Rao, A., Shawe-Taylor, J., Mourao-Miranda, J., and Initiative, A. D.: A multiple hold-out framework for sparse partial least squares, J. Neurosci. Methods, 271, 182–194, 2016.

Mosavi, A., Ozturk, P., and Chau, K.: Flood Prediction Using Machine Learning Models: Literature Review, https://doi.org/10.3390/w10111536, 2018.

Motta, M., de Castro Neto, M., and Sarmento, P.: A mixed approach for urban flood prediction using Machine Learning and GIS, Int. J. Disaster Risk Reduct., 56, 102154, https://doi.org/https://doi.org/10.1016/j.ijdrr.2021.102154, 2021.

Nusit, K., Tantanee, S., and Sooraksa, P.: Flood Susceptibility Mapping Using Machine Learning Models with Novel Flood Inventory Sampling Strategies, Sensors Mater., 37, 3829–3839, https://doi.org/10.18494/SAM5586, 2025.

OECD: OECD Review of Risk Management Policies Morocco, Paris, https://doi.org/10.1787/9789264276482, 2017.

Organization, W. M.: Atlas of Mortality and Economic Losses From Weather, Climate and Water-Related Hazards (1970–

https://doi.org/10.5194/egusphere-2026-1001
Preprint. Discussion started: 7 April 2026

2021), 2021.

Pal, K. and Patel, B. V: Data classification with k-fold cross validation and holdout accuracy estimation methods with 5 different machine learning techniques, in: 2020 fourth international conference on computing methodologies and communication (ICCMC), 83–87, 2020.

Pham, B. T., Prakash, I., and Bui, D. T.: Spatial prediction of landslides using a hybrid machine learning approach based on random subspace and classification and regression trees, Geomorphology, 303, 256–270, 2018.

Pourzangbar, A., Oberle, P., Kron, A., and Franca, M. J.: Analysis of the utilization of machine learning to map flood susceptibility, J. Flood Risk Manag., 18, e70042, 2025.

Rahman, A., Shaw, R., Surjan, A., and Parvin, G. A.: 1 - Urban Disasters and Approaches to Resilience, edited by: Shaw, R., Atta-ur-Rahman, Surjan, A., and Parvin, G. A. B. T.-U. D. and R. in A., Butterworth-Heinemann, 1–19, https://doi.org/https://doi.org/10.1016/B978-0-12-802169-9.00001-X, 2016.

Riazi, M., Khosravi, K., Shahedi, K., Ahmad, S., Jun, C., Bateni, S. M., and Kazakis, N.: Enhancing flood susceptibility modeling using multi-temporal SAR images, CHIRPS data, and hybrid machine learning algorithms, Sci. Total Environ., 871, 162066, 2023.

Sarti, O., Otal, E., Morillo, J., and Ouassini, A.: Integrated assessment of groundwater quality beneath the rural area of R'mel, Northwest of Morocco, Groundw. Sustain. Dev., 14, 100620, 2021.

Sellami, E. M., Maanan, M., and Rhinane, H.: Performance of machine learning algorithms for mapping and forecasting of flash flood susceptibility in Tetouan, Morocco, Int. Arch. Photogramm. Remote Sens. Spat. Inf. Sci., 46, 305–313, 2022.

Shmueli, G.: To explain or to predict?, 2010.

Svetlana, D., Radovan, D., and Ján, D.: The economic impact of floods and their importance in different regions of the world with emphasis on Europe, Procedia Econ. Financ., 34, 649–655, 2015.

Syarifudin, A., Satyanaga, A., and Destania, H. R.: Application of the HEC-RAS Program in the Simulation of the Streamflow Hydrograph for Air Lakitan Watershed, https://doi.org/10.3390/w14244094, 2022.

Tanner, E. M., Bornehag, C.-G., and Gennings, C.: Repeated holdout validation for weighted quantile sum regression, MethodsX, 6, 2855–2860, 2019.

Tazmul Islam, M. and Meng, Q.: An exploratory study of Sentinel-1 SAR for rapid urban flood mapping on Google Earth Engine, Int. J. Appl. Earth Obs. Geoinf., 113, 103002, https://doi.org/10.1016/j.jag.2022.103002, 2022.

Tellman, B., Sullivan, J. A., Kuhn, C., Kettner, A. J., Doyle, C. S., Brakenridge, G. R., Erickson, T. A., and Slayback, D. A.: Satellite imaging reveals increased proportion of population exposed to floods, Nature, 596, 80–86, https://doi.org/10.1038/s41586-021-03695-w, 2021.

Tepetidis, N., Benekos, I., Iliopoulou, T., Dimitriadis, P., and Koutsoyiannis, D.: Combining Machine Learning Models and Satellite Data of an Extreme Flood Event for Flood Susceptibility Mapping, Water (Switzerland), 17, 1–31, https://doi.org/10.3390/w17182678, 2025.

Tramblay, Y.: Modélisation des crues dans le bassin du barrage Makhazine, Maroc, Inst. Rech. pour le Développement Hydrosci. Fr., 2012.

Tupas, M. E., Roth, F., Bauer-Marschallinger, B., and Wagner, W.: An intercomparison of Sentinel-1 based change detection algorithms for flood mapping, Remote Sens., 15, 1200, 2023.

UNDRR, C. and: The Human Cost of Disasters-An overview of the last 20 years 2000-2019, 2020.

Vargas-Yáñez, M., Moya, F., García-Martínez, M. del C., Tel, E., Zunino, P., Plaza, F., Salat, J., Pascual, J., López-Jurado, J. L., and Serra, M.: Climate change in the Western Mediterranean sea 1900–2008, J. Mar. Syst., 82, 171–176, 2010.

Wagner, W., Bauer-Marschallinger, B., Roth, F., and others: The fully-automatic Sentinel-1 Global Flood Monitoring service: Scientific challenges and future directions, Remote Sens. Environ., 333, 115108, https://doi.org/10.1016/j.rse.2025.115108, 2026.

https://doi.org/10.5194/egusphere-2026-1001
Preprint. Discussion started: 7 April 2026

Wahba, M., Essam, R., El-Rawy, M., Al-Arifi, N., Abdalla, F., and Elsadek, W. M.: Forecasting of flash flood susceptibility mapping using random forest regression model and geographic information systems, Heliyon, 10, 2024.

Wahl, T., Jain, S., Bender, J., Meyers, S. D., and Luther, M. E.: Increasing risk of compound flooding from storm surge and rainfall for major US cities, Nat. Clim. Chang., 5, 1093–1097, https://doi.org/10.1038/nclimate2736, 2015.

Ward, P. J., Couasnon, A., Eilander, D., Haigh, I. D., Hendry, A., Muis, S., Veldkamp, T. I. E., Winsemius, H. C., and Wahl, T.: Dependence between high sea-level and high river discharge increases flood hazard in global deltas and estuaries, Environ. Res. Lett., 13, 084012, https://doi.org/10.1088/1748-9326/aad400, 2018.

Wood, H. M. and Lauritson, L.: The CEOS disaster management support group, in: IGARSS 2000. IEEE 2000 International Geoscience and Remote Sensing Symposium. Taking the Pulse of the Planet: The Role of Remote Sensing in Managing the Environment. Proceedings (Cat. No. 00CH37120), 2690–2692, 2000.

Zhao, J., Xiong, Z., and Zhu, X. X.: UrbanSARFloods: Sentinel-1 SLC-Based Benchmark Dataset for Urban and Open-Area Flood Mapping, IEEE Comput. Soc. Conf. Comput. Vis. Pattern Recognit. Work., 419–429, https://doi.org/10.1109/CVPRW63382.2024.00047, 2024.